THE JOURNAL OF PHYSICAL CHEMISTRY C

Article

pubs.acs.org/JPCC

Raman Spectra and Corresponding Strain Effects in Graphyne and Graphdiyne

Shuqing Zhang,[†,‡] Jinying Wang,[†] Zhenzhu Li,[†,‡] Ruiqi Zhao,[§] Lianming Tong,[†] Zhongfan Liu,[†,‡] Jin Zhang,[*,†,‡] and Zhirong Liu[*,†,‡]

[†]Center for Nanochemistry, College of Chemistry and Molecular Engineering and [‡]Academy for Advanced Interdisciplinary Studies, Peking University, Beijing 100871, P. R. China

[§]School of Physics and Chemistry, Henan Polytechnic University, Henan 454003, China

Supporting Information

ABSTRACT: We systematically studied the Raman spectra of graphyne (GY) and graphdiyne (GDY), analyzing their features under mechanical strain by group theory and first-principles calculations. The G bands in GY and GDY were softened compared with that in graphene, which provides a fingerprint useful in detecting their synthesis. We established a unified formulation to describe the effects of both uniaxial and shear strains, and combined this with calculated results to reveal the relationship underlying the changes in Raman evolution under various strains. Each doubly degenerate mode splits into two branches under strain, both of which are red-shifted with tensile uniaxial strain, but one is red-shifted and the other is blue-shifted under shear strain. The splitting under shear strain is double that under uniaxial strain.

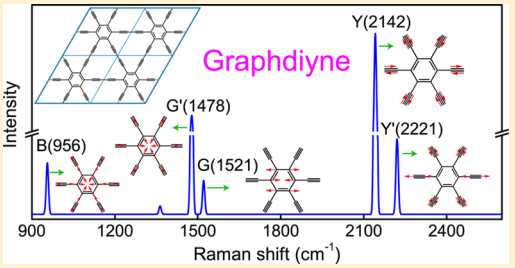

1. INTRODUCTION

Silicon-based semiconductor devices are the basis of modern electronics, but innovation in silicon is approaching its physical limits.[1] To overcome the current limits, much work has been done to seek alternative materials, among which nanocarbon materials—such as carbon nanotubes, graphene—are the most promising candidates.[2−4] Recently, graphyne (GY) and graphdiyne (GDY) have become the focus of these investigations owing to their intriguing mechanical, optical, and electrical properties.[5−7] According to theoretical studies, single-atomic-layer GY and GDY are semiconductors, the band gaps of GY and GDY are close to 0.47 and 0.52 eV through the Perdew−Burke−Ernzerhof (PBE) functional,[8,9] and the more compelling results are found to be 2.23 and 1.18 eV using hybrid functional B3LYP.[9−11] More importantly, the hole and electron carrier mobilities of these carbon allotropes are predicted to be 10^4−10^5 cm^2 V^{-1} s^{-1} at room temperature,[12,13] far exceeding those of silicon. This attractive band gap and high mobility indicate that GY and GDY show promise in future carbon-based electronic devices. Besides, the mechanical properties of GY and GDY have been reported to meet industrial requirements,[14−16] and their nonlinear optical properties would extend the applications of carbon allotropes.[17] GY and GDY are also explored for their applications as catalysts for different important reactions.[18−20]

Experimentally, the syntheses of GY and GDY offer more possibilities compared to other 2D materials containing sp-hybridized carbon atoms. GY was first proposed in 1987 by Baughman et al. in a systematic consideration of new forms of carbon that had been sporadically reported,[21] and GDY is a natural extension of GY. Current synthesis strategies for GY and DGY are mainly based on powerful organometallic synthetic methodologies.[22−24] The largest GY fragments yet to be produced were composed of four monomer molecules.[25] Li et al. synthesized large-area, multilayer GDY films on copper substrates via a cross-coupling reaction using hexaethynylbenzene.[26] Since then, GDY nanotubes and nanowalls have also been fabricated.[27−29] These advances suggest that GY and GDY are likely to be available in significant quantities for use in experimental studies and potential applications.

For the studies of a new material, efficient characterization methods are requisite. In characterizing previous graphitic materials, Raman spectroscopy has exhibited remarkable advantages.[30,31] For example, the positions, intensities, and shapes of Raman bands offer rich information in graphene-related systems.[30] Naturally, one might expect Raman spectroscopy to be a versatile tool in studying GY and GDY. Indeed, Raman has been applied in experimentally characterizing GDY.[26,28] In interpreting Raman signals to gain structural information, theoretical knowledge is valuable; however, there are few theoretical studies on using Raman spectroscopy to investigate GY and GDY.[32] The Raman features of GY have been studied within a nonorthogonal tight-binding (NTB) model.[32] By rationalizing the vibrational modes of various oligomers, the Raman spectrum of a hypothetical 2D sp−sp^2 carbon sheet has also been predicted.[33] Note that their adopted approach was either semiempirical or extrapolative. Moreover, for the only form of synthesized GDY so far, there is no

Received: December 18, 2015
Revised: March 1, 2016
Published: April 25, 2016

DOI: 10.1021/acs.jpcc.5b12388
J. Phys. Chem. C 2016, 120, 10605−10613

theoretical work on its Raman properties. Thus, one motivation of the present study is to investigate the Raman characteristics of GY and GDY through a direct first-principles approach.

Another motivation of this work lies in the strain effect. In the past decade, because of successes in using strain to improve carrier mobility in microelectronics, strain engineering of advanced electronic devices is now an active research field.[34,35] With important advances in motion detections, flexible devices, and wearable sensors, strain engineering is expected to play a more important role in future devices. Straining a system affects its Raman spectrum, which allows one to measure the uniaxial or biaxial strain, providing a fundamental tool for nanoelectronics.[31,36] The effects of strain on the mechanical and electronic properties of GY and GDY have been investigated theoretically,[11,15,16] but their effects on vibrational features remain unexplored.

In the present paper, we studied the Raman spectra of GY and GDY and their dependence on strain. First, we calculated the phonon dispersions of GY and GDY; we found no imaginary phonon mode, verifying the kinetic stability of the phases. Second, we specified the Raman spectra and corresponding lattice vibrational modes of GY and GDY. Third, we determined the elastic properties of graphene, GY, and GDY under strain. Finally, we explored the regularities of Raman bands with applied mechanical strain with considering the effects of both uniaxial and shear strains. We provided a unified formulation to describe the roles of uniaxial and shear strains, which is applicable to other materials with honeycomb symmetry.

2. METHODS

The density functional theory (DFT) calculations were performed using the QUANTUM ESPRESSO package.[37] We used plane-wave basis sets, norm-conserving pseudopotentials generated from the valence configuration of $2s^2 2p^2$ for carbon, and the local density approximation (LDA) for the exchange-correlation function. The structures were fully relaxed to the local minimum, and then the phonon dispersions and Raman spectra were calculated by density functional perturbation theory,[38] which allows one to calculate the phonon frequencies and eigenvectors at any wavevector without using a supercell. The accuracy of the calculations has been verified by a number of experiments.[38,39] To obtain converged results, the kinetic energy cutoffs for wave functions were taken as 100 Ry, corresponding to 400 Ry for the charge density cutoffs. The Brillouin zones were sampled with $12 \times 12 \times 1$ **k**-point meshes in structure optimization calculations. The dynamical matrices of phonons were calculated on $3 \times 3 \times 1$ **q**-grids. The structures were relaxed until all components of all forces were smaller than 0.002 Ry/Bohr. Interlayer interactions were eliminated by setting the interlayer vacuum intervals of all structures to at least 10 Å.

3. RESULTS AND DISCUSSION

3.1. Phonon Dispersion. Figure 1 shows the systems we investigated: graphene, GY, and GDY. They share a common hexagonal structure (Figure 1a), where GY and GDY can be viewed as the results of replacing one-third of the aromatic bonds (dotted lines in Figure 1a) in graphene with acetylenic and diacetylenic groups, respectively. GY and GDY were chosen because their structures are similar to graphene's and GDY films have been synthesized experimentally. The GY system considered here is sometimes named γ-graphyne in some references to avoid confusion with other forms.[40,41]

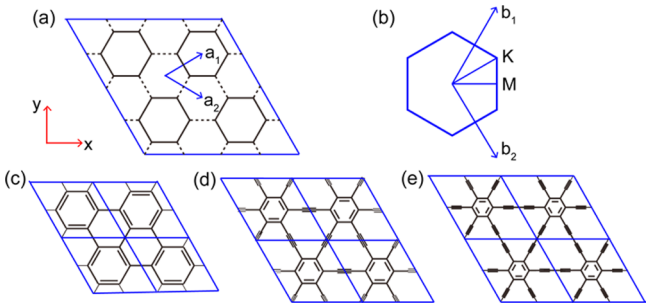

Figure 1. Studied systems with hexagonal symmetry. (a) Schematic representation of the common hexagonal structure with two kinds of bonds (represented by solid and dotted lines, respectively). (b) First Brillouin zone with high-symmetry points. Specific systems considered in this study include (c) graphene, (d) GY, and (e) GDY.

The optimized lattice constants are 2.44 Å for graphene, 6.81 Å for GY, and 9.37 Å for GDY, which agree well with previous calculations (2.43 Å for graphene;[36] 6.83 and 6.86 Å for GY;[42,43] 9.38 and 9.44 Å for GDY[42,43]). Figure 2 shows the phonon dispersions and vibrational density of states. GY has 12 atoms and GDY has 18 atoms in the primitive cells, so GY has 36 vibrational modes and GDY has 54. No imaginary phonon mode appeared in the three systems, further supporting their mechanical and kinetic stability.

3.2. Raman Spectra and Symmetry Analysis. The monolayer graphene, GY, and GDY have the same hexagonal symmetry, taking on the two-dimensional space-group *P6/mmm* (D_{6h}^1) in the Hermann–Mauguin (Schoenflies) notation.[44] For the first-order Raman scattering considered here, the scattering process is limited to phonons at the Brillouin zone center Γ point with D_{6h} symmetry owing to the law of momentum conservation. The irreducible representations of optical modes at the zone center are given as follows (while the acoustic modes are $A_{2u} + E_{1u}$):

$$\begin{cases} \Gamma_{\text{graphene}} = B_{2g} + E_{2g} \\ \Gamma_{\text{GY}} = A_{2u} + 3E_{1u} + 2B_{1u} + 2B_{2u} + 2E_{2u} + 2A_{1g} + 2A_{2g} + 2B_{1g} + 2E_{1g} + 4E_{2g} \\ \Gamma_{\text{GDY}} = 2A_{2u} + 5E_{1u} + 3B_{1u} + 3B_{2u} + 3E_{2u} + 3A_{1g} + 3A_{2g} + 3B_{1g} + 3E_{1g} + 6E_{2g} \end{cases} \quad (1)$$

where A_{1g}, E_{1g}, and E_{2g} are Raman-active modes, and A_{2u} and E_{1u} are infrared-active modes. Tables 1 and Table 2 give details on the assignments and related properties for GY and GDY.

For graphene, the only Raman-active mode is assigned to the doubly degenerate representation E_{2g}, which corresponds to the G band in graphene and is related to the C═C aromatic stretching mode. The calculated frequency in our study is 1620 cm^{-1}, which is slightly larger than the experimental value of 1580 cm^{-1}.[30] The discrepancy is mainly caused by the tiny underestimate in bond length (2.44 Å) by the LDA calculation compared with the experiment result (2.46 Å). If we adopted a lattice constant of 2.46 Å, the calculated frequency would red-shift to 1572 cm^{-1}, almost identical to the experimental value.

For GY and GDY, the calculated Raman spectra and atomic motions of vibrational modes are presented in Figure 3 and Figure 4, respectively. The analysis of atomic motion focused

DOI: 10.1021/acs.jpcc.5b12388
J. Phys. Chem. C 2016, 120, 10605−10613

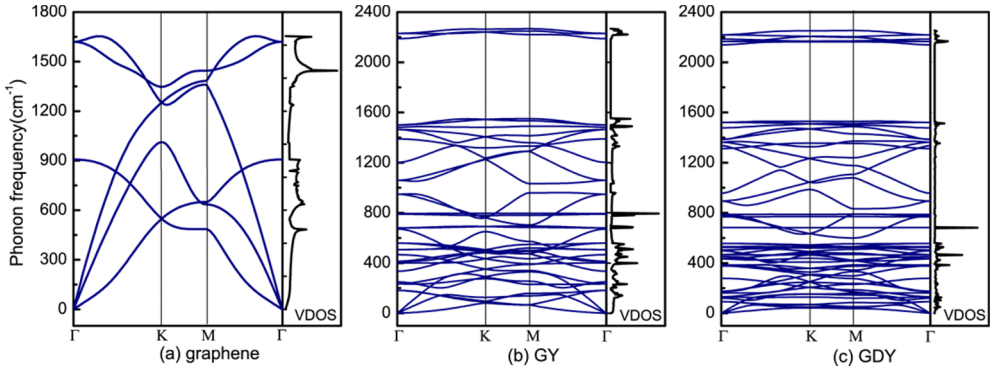

Figure 2. Phonon dispersions and vibrational density of states (VDOS) for (a) graphene, (b) GY, and (c) GDY.

Table 1. Mode Assignments and Related Properties at the Γ Point for GY[a]

freq (cm^{-1})	irreps	RRI	freq (cm^{-1})	irreps	RRI
0	A_{2u}		680	E_{2u}	
0	E_{1u}		789	A_{2g}	
183	E_{2u}		795	B_{1g}	
234	E_{1g} [R]	1×10^{-8}	948	E_{2g} [R]	1×10^{-4}
250	A_{2g}		1059	E_{1u} [I]	
336	A_{2u} [I]		1202	A_{1g} [R]	0.3
401	B_{1u}		1388	B_{1u}	
414	E_{1u} [I]		1464	E_{2g} [R]	0.004
467	B_{1g}		1480	B_{2u}	
507	E_{2g} [R]	1×10^{-4}	1500	E_{1u} [I]	
559	E_{1g} [R]	1×10^{-6}	2187	A_{1g} [R]	1.0
670	B_{2u}		2229	E_{2g} [R]	1×10^{-5}

[a]Phonon frequencies (freq), irreducible representations (irreps) with indicated Raman/infrared activities ([R]/[I]), and relative Raman intensities (RRI) normalized by the largest value.

Table 2. Mode Assignments and Related Properties at the Γ Point for GDY[a]

freq (cm^{-1})	irreps	RRI	freq (cm^{-1})	irreps	RRI
0	A_{2u}		529	E_{2g} [R]	1×10^{-4}
0	E_{1u}		556	E_{1g} [R]	1×10^{-6}
94	E_{2u}		684	E_{2u}	
119	E_{1g} [R]	1×10^{-8}	769	A_{2g}	
132	A_{2g}		774	E_{2g} [R]	1×10^{-5}
161	B_{1u}		788	B_{1g}	
172	A_{2u} [I]		894	E_{1u} [I]	
176	E_{1u} [I]		956	A_{1g} [R]	0.08
282	B_{1g}		1313	B_{1u}	
377	E_{2u}		1335	B_{2u}	
383	E_{2g} [R]	1×10^{-4}	1364	E_{2g} [R]	0.006
434	E_{1g} [R]	1×10^{-8}	1385	E_{1u} [I]	
449	E_{1u} [I]		1478	A_{1g} [R]	0.3
466	A_{2u} [I]		1521	E_{2g} [R]	0.03
467	B_{1u}		2142	A_{1g} [R]	1
498	B_{2u}		2168	E_{1u} [I]	
505	A_{2g}		2187	B_{2u}	
526	B_{1g}		2221	E_{2g} [R]	0.06

[a]Phonon frequencies (freq), irreducible representations (irreps) with indicated Raman/infrared activities ([R]/[I]), and relative Raman intensities (RRI) normalized by the largest value.

on the relatively intense Raman lines (RRS > 0.001), which are located in the high-frequency regions. We name these peaks as

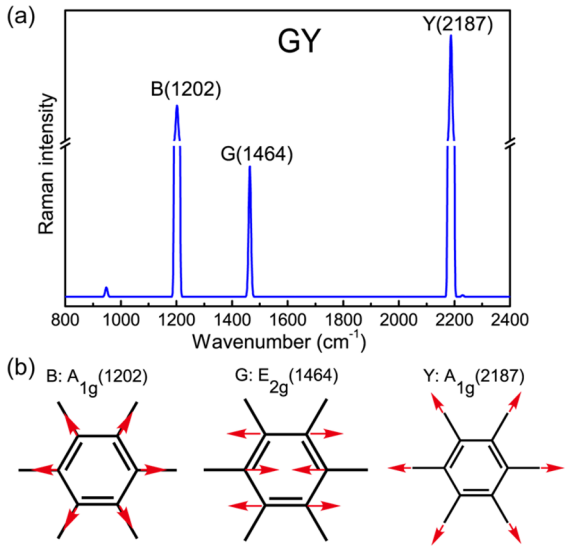

Figure 3. Raman spectra and vibrational modes of GY. (a) Predicted Raman spectrum, whose peaks are with 10 cm^{-1} Gaussian smearing. (b) Atomic motions of intense Raman-active modes, in which the red arrows show the motion directions of the main contributors.

follows: the breathing vibration is B, the vibrations related to sp^2 carbon are G, G′, and G″ (similar to other sp^2 materials), and the alkyne-related modes are Y and Y′, respectively. The Raman intensities are normalized by the largest values in each system. Characteristic groups have their unique vibrational modes, such as the stretching, scissoring of aromatic bonds, and triple bonds. However, it should also be noted that they are all coupled with the surroundings, causing the frequencies to shift slightly. Generally speaking, vibrational modes are very complicated from the perspective of vibration vectors. Our assignments only consider the main contributors to these modes.

The predicted Raman spectrum of GY has three major peaks (Figure 3), consistent with the result given by the NTB model.[32] An extraordinary feature is the softening of the G band (1464 cm^{-1}) compared with that of graphene (1620 cm^{-1} in our calculation and 1580 cm^{-1} in experiments), which would be useful in detecting the synthesis of GY. NTB model usually overestimates phonon frequencies compared with the experimental values in the high-frequency region, while it underestimates them in low-frequency region,[32,45] so it is good to have a quantitative comparison between our DFT results and those given by NTB. In the high-frequency region above 1000 cm^{-1}, the NTB values (1221, 1518, 2258, 2272 cm^{-1}) are

DOI: 10.1021/acs.jpcc.5b12388
J. Phys. Chem. C 2016, 120, 10605−10613

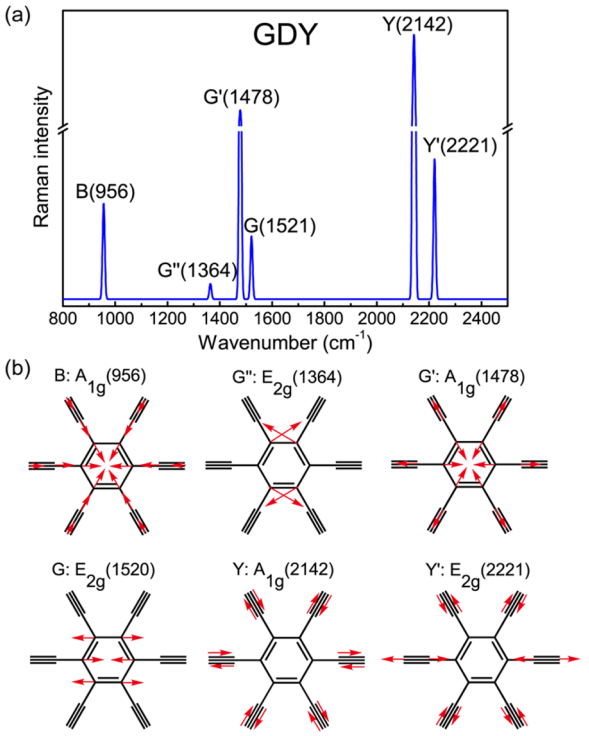

Figure 4. Raman spectra and vibrational modes of GDY. (a) Predicted Raman spectrum, whose peaks are with 10 cm^{-1} Gaussian smearing. (b) Atomic motions of intense Raman-active modes, in which the red arrows show the motion directions of the main contributors.

consistently larger than our DFT values in Table 1 (1202, 1464, 2187, 2229 cm^{-1}). In the low-frequency region below 1000 cm^{-1}, the NTB values (417, 906 cm^{-1}) are consistently smaller than our DFT values (507, 948 cm^{-1}). Thus, the systematic deviation of the NTB model in the high-frequency region is indeed different from that in the low-frequency region, as discussed in the case of C_{60}.[45]

Compared with GY, GDY has more atoms in a primitive cell, so it has more complicated vibrational modes. Specifically, GDY has six intense Raman peaks, three of which are similar to those in GY: the B peak mainly comes from the breathing vibration of benzene ring and alkyne-related ring; the G peak mostly comes from stretching of aromatic bonds as in graphene, and the wavenumber and intensity of this mode is relatively small in these alkyne-rich 2D systems, suggesting it ought to be a general feature of GY and GDY with the introduction of acetylenic linkages; the Y peak comes from the synchronous stretching/contracting of triple bonds, which is a fully symmetric mode. The other three intense Raman-active peaks are observed in only GDY. The G″ peak is ascribed to the scissoring vibration of atoms in benzene ring. The G′ peak comes from the vibrations of C−C bonds between triply coordinated atoms and theirs doubly coordinated neighbors. Unexpectedly, G′ is even stronger than G. The Y′ peak is another stretching mode of alkyne triple bonds, but the vibrations of different triple bonds are out-of-phase: one-third of triple bonds are stretching while the remaining two-thirds are contracting, as shown in Figure 4b.

In an earlier work, Raman spectra of some oligomers with similar structures have been calculated.[33] The oligomers therein are homocoupling products of 1,3,5-triethynylbenzene (TEB), which has three alkynes around benzene. The 2D network of TEB has hydrogens. In comparison, GY and GDY investigated here have denser carbon atoms and stronger conjugated effects. It was found that the G band of oligomers changed slightly with increasing polymerization degree, and the G band of the 2D network of TEB was estimated to be 1560 cm^{-1}.[33] In the current work, the G band of GY and GDY is distinctly smaller, i.e., 1464 cm^{-1} in GY and 1520 cm^{-1} in GDY, which reflects the influence of conjugated effects.

Experimentally, controlled syntheses of GY and GDY are still in the very early stages. Constructing regular 2D all-carbon structures by organometallic synthetic method remains extremely difficult because of uncontrollable side reactions.[33,46] GY has not been produced in significant scales to date. For GDY, although the monolayer sample is not available yet, large-area-multilayer films[26] and nanowalls[28] have been produced by metal catalyzed cross-coupling reactions in solution. Therefore, here we compare the calculated and experimental Raman spectra of GDY. The Raman bands of the GDY samples are broad, likely because the accessible crystallized areas are not large enough. In the experimental sample, a peak at around 1570 cm^{-1} is accompanied by a lower-frequency shoulder at around 1380 cm^{-1}; the latter is absent in conventional carbon materials. Comparing these results with the calculated results, we roughly attribute the experimental peaks between 1380 and 1570 cm^{-1} to the G″, G′, and G peaks shown in Figure 4. The experimental peak near 2180−2190 cm^{-1} can be attributed to Y and Y′, which are specific to alkyne-related stretching vibrations.

The most puzzling peak in experiments is that observed near 1930−1940 cm^{-1}. It has appeared in many experimental studies on alkyne materials,[47,48] but its interpretation is still somewhat controversial. Some papers have explained it as the presence of an important fraction of cumulene carbon chains (cumulene-like at 1959 cm^{-1}),[48−50] although thermodynamic calculations show that polyyne carbon should be more stable than cumulene carbon (polyyne-like at about 2100 cm^{-1}).[43,51] Another explanation points to copper(I) acetylide analogs (the −C≡C− vibration of $C_6H_5C{\equiv}CCu$ at 1926−1953 cm^{-1}).[47] Regardless, there is no intrinsic Raman band predicted in this region for GY and GDY (Figures 3 and 4), so the observed band here likely comes from byproducts or intermediates.

3.3. Elastic Properties. Before discussing the behaviors of the Raman spectrum in strained samples, we will first briefly survey the mechanical properties of the studied systems. GY and GDY have the same hexagonal symmetry as graphene, so they have isotropic elastic properties under small deformation.[52] For a hexagonal structure, it has four nonzero second-order elastic constants in 2D systems, i.e., C_{11}, C_{12}, C_{22}, C_{66} (using the conventional Voigt notation[53]), which satisfy $C_{11} = C_{22}$, $C_{66} = (C_{11} - C_{12})/2$. For 2D systems, the Poisson's ratio ν, in-plane Young's modulus Y, and shear modulus G may be obtained by the following relationships: $\nu = C_{12}/C_{11}$, $Y = (C_{11}^2 - C_{12}^2)/C_{11} = C_{11}(1 - \nu^2)$, $G = C_{66}$. Table 3 summarizes our calculated results, which agree well with values from the literature, also listed for comparison.

The Poisson's ratio ν is the negative ratio of transverse to axial strain, which characterizes a material's ability to deform under uniaxial strain. The ν values of GY and GDY are more than twice as large as that of graphene, probably because their long alkyne linkages are more likely to bend under uniaxial strain. There is also significant decrease in the Young's and shear moduli from graphene to GY to GDY. The in-plane Young's modulus, representing a material's stiffness, of GY and

DOI: 10.1021/acs.jpcc.5b12388
J. Phys. Chem. C 2016, 120, 10605−10613

Table 3. Elastic Properties for Graphene, GY, and GDY, Including Elastic Constants C_{11} and C_{12}, Poisson's Ratio ν, Shear Modulus G, and in-Plane Young's Modulus Y

	C_{11} (N/m)	C_{12} (N/m)	ν	Y (N/m)	G (N/m)
Graphene[a]	368.8	66.50	0.180	356.9	151.2
Graphene[55]	358.1	60.40	0.169	348.0	148.9
GY[a]	207.7	92.42	0.445	166.6	57.64
GY[15]	198.7	85.30	0.429	162.1	56.70
GDY[a]	159.0	72.67	0.457	125.8	43.18
GDY[56]	152.1	69.00	0.454	120.8	41.60

[a]Calculated by this work.

GDY are 46.7% and 35.2% of graphene's, respectively. This result indicates that the structures of GY and GDY are more sensitive to strain than graphene. In addition, the shear moduli of GY and GDY are only about one-third of graphene's, showing that they experience more bond bending under shear strain, which is consistent with a previous theoretical prediction.[13] Currently only graphene has elastic study in experiment, and our 2D Young's modulus (356.9 N m^{-1}) agrees well with experimental data (340 ± 50 N m^{-1}).[54]

3.4. Strain Dependence of Raman Bands. In this section, we will discuss the detailed Raman shifts of graphene, GY, and GDY as functions of mechanical strain. The applied strain tensor is written as

$$\varepsilon = \begin{bmatrix} \varepsilon_{xx} & \varepsilon_{xy} \\ \varepsilon_{xy} & \varepsilon_{yy} \end{bmatrix} = \begin{bmatrix} \varepsilon_{xx} & 0 \\ 0 & 0 \end{bmatrix} + \begin{bmatrix} 0 & 0 \\ 0 & \varepsilon_{yy} \end{bmatrix} + \begin{bmatrix} 0 & \varepsilon_{xy} \\ \varepsilon_{xx} & 0 \end{bmatrix} \quad (2)$$

where the first and second terms on the right side of the equation represent the uniaxial strain along the x and y directions, respectively, while the third term is the tensorial shear strain component. The Raman frequency ω can be viewed as a function of strain. If the applied strain is small enough, the high-order effect can be ignored. Thus, here we focus on the linear effect of ε on ω.

When the vibrational mode is nondegenerate, the frequency ω as a function of strain ε can be generally expanded as a Taylor series:

$$\omega(\varepsilon_{xx}, \varepsilon_{yy}, \varepsilon_{xy}) = \omega_0 + \alpha\varepsilon_{xx} + \beta\varepsilon_{yy} + \chi\varepsilon_{xy} + (\text{higher order terms}) \quad (3)$$

where α, β, and χ are the linear coefficients. As discussed above, graphene, GY, and GDY have the same hexagonal symmetry, which is isotropic in two dimensions. As such the coefficients satisfy $\alpha = \beta$ (= $\bar{\alpha}$ in a symbol style similar to the degenerate case below). By applying different sets of (ε_{xx}, ε_{yy}, ε_{xy}), it is simple to determine α, β, and χ.

When the vibrational mode is doubly degenerate, under strain it will split into two bands. The energies of splitting modes are the eigenvalues of the corresponding Hamiltonian, which can be written as

$$\mathrm{H} = \begin{bmatrix} a & c \\ c & b \end{bmatrix} \quad (4)$$

in which only two bands are considered. The solutions are given as

$$\omega_{1,2} = \frac{(a+b) \pm \sqrt{(a-b)^2 + 4c^2}}{2} \quad (5)$$

The conditions to the degenerate in unstrained sample are $a = b = a_0$, $c = 0$, so a, b, c under small strain can be expanded as

$$\begin{cases} a = a_0 + \alpha_1\varepsilon_{xx} + \beta_1\varepsilon_{yy} + \chi_1\varepsilon_{xy} \\ b = a_0 + \alpha_2\varepsilon_{xx} + \beta_2\varepsilon_{yy} + \chi_2\varepsilon_{xy} \\ c = \alpha_3\varepsilon_{xx} + \beta_3\varepsilon_{yy} + \chi_3\varepsilon_{xy} \end{cases} \quad (6)$$

The detailed process to solve the relationships among a, b, and c under hexagonal symmetry are given in the Supporting Information. As a result, the universal rule of a doubly degenerate mode with strain is deduced out to be

$$\omega_{1,2} = \omega_0 + \bar{\alpha}(\varepsilon_{xx} + \varepsilon_{yy}) \pm \Delta\alpha\sqrt{(\varepsilon_{xx} - \varepsilon_{yy})^2 + 4\varepsilon_{xy}^2} \quad (7)$$

where $\bar{\alpha} = \frac{\alpha_1 + \alpha_2}{2} = \frac{\beta_1 + \beta_2}{2}$ and $\Delta\alpha = \frac{\alpha_1 - \alpha_2}{2} = \frac{\beta_1 - \beta_2}{2}$. If only uniaxial strains are applied, i.e., $\varepsilon_{xy} = 0$, then eq 7 simplifies to

$$\begin{cases} \omega_1(\varepsilon_{xx}, \varepsilon_{yy}) = \omega_0 + (\bar{\alpha} + \Delta\alpha)\varepsilon_{xx} + (\bar{\alpha} - \Delta\alpha)\varepsilon_{yy} \\ \omega_2(\varepsilon_{xx}, \varepsilon_{yy}) = \omega_0 + (\bar{\alpha} - \Delta\alpha)\varepsilon_{xx} + (\bar{\alpha} + \Delta\alpha)\varepsilon_{yy} \end{cases} \quad (8)$$

Note that the splitting high-frequency and low-frequency vibrational vectors would exchange when ε_{xx} and ε_{yy} are separately applied.

The evolutions of Raman shifts with uniaxial strain for graphene, GY, and GDY were calculated by DFT, and these results are summarized in Figure 5. A strain up to ±4% was considered, and it is noted that the possibility of buckles under a compressive strain (which is likely to occur in experiments) was ignored in the calculations since we adopted a unit cell with the periodic boundary conditions. The calculated data are fitted with a parabolic equation (detailed results are provided in the Supporting Information), and the resulting linear coefficients are listed in Figure 5b–k. The nonlinear effects in GY and GDY are stronger than that in graphene, perhaps because GY and GDY are softer and easier to deform than graphene. Figure S1 shows the variations in bond lengths and angles with uniaxial strain; the variations in bond angles, especially those related to alkyne triple bonds, have large quadratic terms. For a doubly degenerate mode, it splits into two branches, giving four linear coefficients under ε_{xx} and ε_{yy}. Theoretical analysis (eq 8) predicted that four linear coefficients can be grouped into two values, i.e., $\bar{\alpha} + \Delta\alpha$ and $\bar{\alpha} - \Delta\alpha$. The calculations agree well with the prediction. For example, for the G band of GDY (Figure 5i), four obviously separated curves exist under high-order effects, but the linear coefficients ($k_{x+} = -25.8$, $k_{x-} = -38.5$, $k_{y+} = -26.3$, $k_{x-} = -39.9$) are well grouped into two values, ($-25.8 \approx -26.3$ and $-38.5 \approx -39.9$), from which we determined that $\bar{\alpha} = -32.6$ and $\Delta\alpha = 6.6$. For a nondegenerate mode, the theory predicted that the linear coefficients under ε_{xx} and ε_{yy} are equal because the systems are isotropic. For example, the calculation gives $k_x = -26.8 \approx k_y = -26.3$ for the B band in GY. The analyses for other modes are similar. The resulting $\bar{\alpha}$ and $\Delta\alpha$ are summarized in Table 4.

In experiments, to introduce strain into a single-layer sample such as graphene, the layer is usually deposited on a flexible polymer substrate. Then, when the system is stretched with ε in one direction, it will contract with $\nu\varepsilon$ in the perpendicular

DOI: 10.1021/acs.jpcc.5b12388
J. Phys. Chem. C 2016, 120, 10605−10613

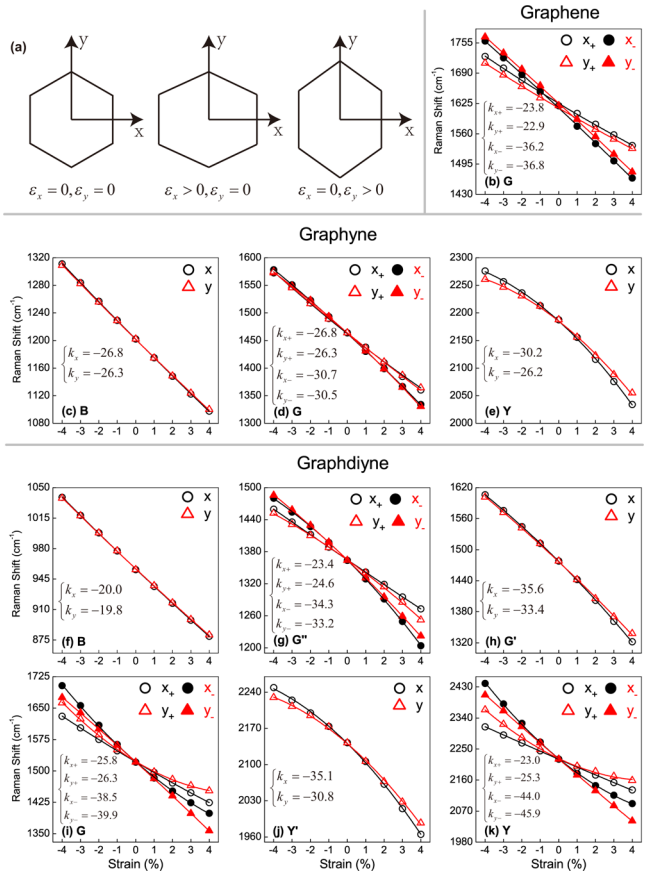

Figure 5. Evolutions of Raman shifts with uniaxial strain for graphene, GY, and GDY. (a) From left to right are the original hexagon and its deformation schematics under uniaxial tensile strain along x axis and y axis. (b) G peak in graphene. (c–e) For GY, with (c) B peak, (d) G peak, and (e) Y peak. (f–k) For GDY, with (f) B peak, (g) G″ peak, (h) G′ peak, (i) G peak, (j) Y peak, and (k) Y′ peak. Raman shifts are given as functions of uniaxial strain [ε_{xx} and ε_{yy}, which are applied separately as illustrated in (a)]. The DFT-calculation data points (squares and triangles) are fitted with a parabolic equation (solid lines), and the resulting first-order (linear) coefficients (k_x, k_y, etc., in units of cm^{-1}/%) are also listed in the panels. Black and red are used for results under ε_{xx} and ε_{yy}, respectively. For the splitting of degenerate bands, the open and filled symbols show the data for the high-frequency and low-frequency bands under tensile strain, respectively.

direction, where ν is the Poisson's ratio of the substrate. Thus, the measured Raman frequency of the deformed sample is given by

$$\omega(\varepsilon) = \omega_{1,2}(\varepsilon, -\nu\varepsilon) \tag{9}$$

where $\omega_{1,2}$ are given in eq 8. The variation of ω with respect to ε are characterized by

$$\begin{cases} \dfrac{\partial\omega_1}{\partial\varepsilon} = (1-\nu)\bar{\alpha} + (1+\nu)\Delta\alpha \\ \dfrac{\partial\omega_2}{\partial\varepsilon} = (1-\nu)\bar{\alpha} - (1+\nu)\Delta\alpha \end{cases} \tag{10}$$

From the parameters in Table 4, we calculated how strain affects the G band of graphene on various substrates and compared these predictions with experimental results, as shown in Table 5. The calculations and experiments agree excellently in most cases. The only mismatch is for the (polydimethylsiloxane) PDMS substrate, which may have been caused by PDMS being too soft, which would likely cause inefficient strain propagation between the graphene and PDMS. Our analysis can be readily extended to GY and GDY, which await validation in future experiments.

We now consider the effect of shear strain. Figure S2 shows the detailed variations in bond lengths and angles under shear strain. Structural relaxation under shear strain is larger than that under uniaxial strain because there are more volatile variables in shear strain. As such, Raman shifts under shear strain are more likely to act nonlinearly, as confirmed by our DFT calculation in Figure 6 (where the strain was restrained to [−3%, + 3%] to reduce errors). While stretching uniaxial strain will always soften Raman modes, shear strain can either soften or harden the modes, which would cause complicated phenomena, as observed in CVD-grown graphene.[60] According to eq 7, the effect of shear strain is closely related to that of uniaxial strain. Specifically, the splitting of doubly degenerate modes under shear strain is given by

$$\frac{\partial(\omega_+ - \omega_-)}{\partial\varepsilon_{xy}} = 4\Delta\alpha \tag{11}$$

where $\Delta\alpha$ was determined in the uniaxial strain effect (Table 4). Table 6 directly compares the calculated $\partial(\omega_+ - \omega_-)/\partial\varepsilon_{xy}$ and the previously determined $4\Delta\alpha$. These agree satisfactorily, supporting the validity of the theory.

At the end of this part, we would like to have a brief discussion on the effects of van der Waals (vdW) interactions, which were usually missed in standard DFT calculations. One of the most popular methods in treating the vdW interactions is nonlocal van der Waals density functional (vdW-DF).[61] We conducted calculations using vdW-DF combined with PBE functional to investigate the effects of vdW interactions. If we constrain the lattice constant of graphene to the experimental value (2.46 Å), the calculated frequencies for G peak are 1572, 1573, and 1589 cm^{-1} by LDA, PBE, and PBE+vdW, respectively. They are all very close to the experimental value of 1580–1589 cm^{-1}.[62] If we optimized the structures in calculations, the obtained frequencies are slightly affected by the methods used, but the red-shift values of G band in GY and GDY with respect to that in graphene are nearly invariable (see Table S3). We also calculated the strain dependence of Raman bands with vdW interactions, and found that the obtained

Table 4. Determined Parameters for the Strain Effects on Raman Bands in Graphene, GY, and GDY[a]

	graphene	GY			GDY					
	G	B	G	Y	B	G″	G′	G	Y	Y′
$\bar{\alpha}$	−29.9	−26.5	−28.5	−28.3	−19.9	−28.9	−34.5	−32.6	−32.9	−34.5
$\Delta\alpha$	6.6	–	2.0	–	–	4.9	–	6.6	–	10.4

[a]in cm^{-1}/% strain.

DOI: 10.1021/acs.jpcc.5b12388
J. Phys. Chem. C 2016, 120, 10605–10613

Table 5. Slopes of Raman Shifts for the Splitting G Modes in Strained Graphene on Various Substrates[a]

	vacuum		PDMS		PET		DFT		
	ref 57	calcd[b]	ref 58	calcd[b]	ref 57	calcd[b]	ref 57	ref 59	calcd[b]
ν	0.13	0.13	0.5	0.5	0.33	0.33	0.164	0.15	0.18
$\partial\omega_1/\partial\varepsilon$	−18.9	−18.7	−5.6	−5.2	−10.8	−11.3	−14.5	−17.0	−16.8
$\partial\omega_2/\partial\varepsilon$	−36.4	−33.5	−12.5	−24.8	−31.7	−28.8	−34.0	−34.0	−32.3

[a]in cm^{-1}/% strain. [b]Calculated by this work.

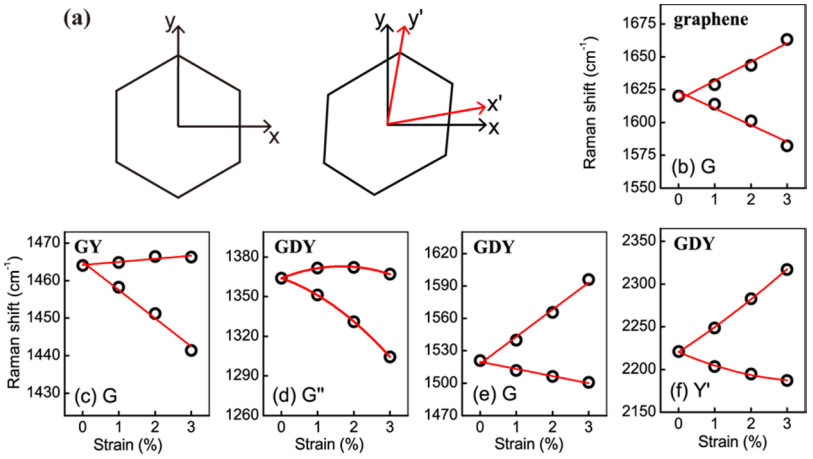

Figure 6. Changes in doubly degenerate Raman modes under shear strain for graphene, GY, and GDY. (a) Schematics of the original hexagon and its deformation under shear strain. (b) G peak in graphene. (c) G peak in GY. (d–f) For GDY, with (d) G″ peak, (e) G peak, (f) Y′ peak. The DFT-calculated data points are fitted with a parabolic equation (in panels (d) and (f)) or a linear equation (in other panels).

Table 6. Splitting of Doubly Degenerate Modes under Shear Strain

	graphene	GY	GDY		
	G	G	G″	G	Y′
$\frac{\partial(\omega_+ - \omega_-)}{\partial\varepsilon_{xy}}$	27.1	8.3	20.2	31.6	45.8
$4\Delta\alpha$	26.4	8.0	19.6	26.4	41.6

slopes between Raman frequencies and the strain are unaffected by the functionals used.

4. CONCLUSIONS

We studied the Raman spectra of GY and GDY and their dependence on strain. The phonon spectra and vibrational density of states were calculated by DFT calculations; these revealed no imaginary phonon mode, giving evidence for these systems' mechanical and kinetic stability. The Raman spectra and atomic motions of intense vibrational modes were determined, and the G bands in GY and GDY were found to be softened compared with that in graphene, which would be a useful way to detect their synthesis. We deduced theoretical equations according to the group theory to provide a unified description of various strain effects on the Raman spectrum, and we used this description to analyze the DFT-calculated results of graphene, GY, and GDY. When uniaxial strain is applied, all Raman bands red-shifted, and doubly degenerate modes split. The calculated shifts of the G mode of graphene deposited on various substrates are consistent with previous experiments. When shear strain is applied, the doubly degenerate modes also split, each with one splitting branch red-shifted and one blue-shifted. The inherent relationship between changes in Raman shifts and applied uniaxial and shear strains will help in the characterization and fabrication of nanoelectronic devices.

■ ASSOCIATED CONTENT

Supporting Information

The Supporting Information is available free of charge on the ACS Publications website at DOI: 10.1021/acs.jpcc.5b12388.

Detailed deduction process of equations and the variations of bond lengths and angles under mechanical strain (PDF)

■ AUTHOR INFORMATION

Corresponding Authors

*E-mail: jinzhang@pku.edu.cn.

*E-mail: LiuZhiRong@pku.edu.cn.

Author Contributions

The manuscript was written through contributions of all authors. All authors have given approval to the final version of the manuscript. The authors declare no competing financial interest.

Notes

The authors declare no competing financial interest.

■ ACKNOWLEDGMENTS

We thank Jingyuan Zhou, Rong Liu, Xin Gao, and Ziqian Xie for valuable discussions. The work was supported by the National Natural Science Foundation of China (No. 21373015, 51432002, 21129001, 21233001).

■ REFERENCES

(1) Keyes, R. W. Physical Limits of Silicon Transistors and Circuits. *Rep. Prog. Phys.* **2005**, *68*, 2701–2746.

DOI: 10.1021/acs.jpcc.5b12388
J. Phys. Chem. C 2016, 120, 10605–10613

(2) Hirsch, A. The Era of Carbon Allotropes. *Nat. Mater.* **2010**, *9*, 868−871.
(3) Iijima, S. Helical Microtubules of Graphitic Carbon. *Nature* **1991**, *354*, 56−58.
(4) Novoselov, K. S.; Geim, A. K.; Morozov, S. V.; Jiang, D.; Zhang, Y.; Dubonos, S. V.; Grigorieva, I. V.; Firsov, A. A. Electric Field Effect in Atomically Thin Carbon Films. *Science* **2004**, *306*, 666−669.
(5) Li, Y.; Xu, L.; Liu, H.; Li, Y. Graphdiyne and Graphyne: From Theoretical Predictions to Practical Construction. *Chem. Soc. Rev.* **2014**, *43*, 2572−2586.
(6) Wang, J. Y.; Deng, S. B.; Liu, Z. F.; Liu, Z. R. The Rare Two-Dimensional Materials with Dirac Cones. *Natl. Sci. Rev.* **2015**, *2*, 22−39.
(7) Ivanovskii, A. L. Graphynes and Graphdyines. *Prog. Solid State Chem.* **2013**, *41*, 1−19.
(8) Perdew, J. P.; Burke, K.; Ernzerhof, M. Generalized Gradient Approximation Made Simple. *Phys. Rev. Lett.* **1996**, *77*, 3865−3868.
(9) Srinivasu, K.; Ghosh, S. K. Graphyne and Graphdiyne: Promising Materials for Nanoelectronics and Energy Storage Applications. *J. Phys. Chem. C* **2012**, *116*, 5951−5956.
(10) Lee, C.; Yang, W.; Parr, R. G. Development of the Colle-Salvetti Correlation-Energy Formula into a Functional of the Electron Density. *Phys. Rev. B: Condens. Matter Mater. Phys.* **1988**, *37*, 785−789.
(11) Xi, J.; Wang, D.; Shuai, Z. Electronic Properties and Charge Carrier Mobilities of Graphynes and Graphdiynes from First Principles. *WIREs Comput. Mol. Sci.* **2015**, *5*, 215−227.
(12) Long, M.; Tang, L.; Wang, D.; Li, Y.; Shuai, Z. Electronic Structure and Carrier Mobility in Graphdiyne Sheet and Nanoribbons: Theoretical Predictions. *ACS Nano* **2011**, *5*, 2593−2600.
(13) Li, Z.; Wang, J.; Liu, Z. Intrinsic Carrier Mobility of Dirac Cones: The Limitations of Deformation Potential Theory. *J. Chem. Phys.* **2014**, *141*, 144107.
(14) Cranford, S. W.; Brommer, D. B.; Buehler, M. J. Extended Graphynes: Simple Scaling Laws for Stiffness, Strength and Fracture. *Nanoscale* **2012**, *4*, 7797−7809.
(15) Peng, Q.; Ji, W.; De, S. Mechanical Properties of Graphyne Monolayers: A First-Principles Study. *Phys. Chem. Chem. Phys.* **2012**, *14*, 13385−13391.
(16) Pei, Y. Mechanical Properties of Graphdiyne Sheet. *Phys. B* **2012**, *407*, 4436−4439.
(17) Zhou, Y. F.; Feng, S. Y. Electronic Spectra and Third-Order Nonlinear Properties of New Structures in Carbon Family. *Solid State Commun.* **2002**, *122*, 307−310.
(18) Srinivasu, K.; Ghosh, S. K. Transition Metal Decorated Graphyne: An Efficient Catalyst for Oxygen Reduction Reaction. *J. Phys. Chem. C* **2013**, *117*, 26021−26028.
(19) Yu, H. Z.; Du, A. J.; Song, Y.; Searles, D. J. Graphyne and Graphdiyne: Versatile Catalysts for Dehydrogenation of Light Metal Complex Hydrides. *J. Phys. Chem. C* **2013**, *117*, 21643−21650.
(20) Wu, P.; Du, P.; Zhang, H.; Cai, C. Graphyne-Supported Single Fe Atom Catalysts for Co Oxidation. *Phys. Chem. Chem. Phys.* **2015**, *17*, 1441−1449.
(21) Baughman, R. H.; Eckhardt, H.; Kertesz, M. Structure-Property Predictions for New Planar Forms of Carbon - Layered Phases Containing Sp2 and Sp Atoms. *J. Chem. Phys.* **1987**, *87*, 6687−6699.
(22) Diederich, F. Carbon Scaffolding - Building Acetylenic All-Carbon and Carbon-Rich Compounds. *Nature* **1994**, *369*, 199−207.
(23) Peng, Q.; Dearden, A. K.; Crean, J.; Han, L.; Liu, S.; Wen, X.; De, S. New Materials Graphyne, Graphdiyne, Graphone, and Graphane: Review of Properties, Synthesis, and Application in Nanotechnology. *Nanotechnol., Sci. Appl.* **2014**, *7*, 1−29.
(24) Haley, M. M. Synthesis and Properties of Annulenic Subunits of Graphyne and Graphdiyne Nanoarchitectures. *Pure Appl. Chem.* **2008**, *80*, 519−532.
(25) Tahara, K.; Yamamoto, Y.; Gross, D. E.; Kozuma, H.; Arikuma, Y.; Ohta, K.; Koizumi, Y.; Gao, Y.; Shimizu, Y.; Seki, S.; Kamada, K.; Moore, J. S.; Tobe, Y. Syntheses and Properties of Graphyne Fragments: Trigonally Expanded Dehydrobenzo[12]Annulenes. *Chem. - Eur. J.* **2013**, *19*, 11251−11260.
(26) Li, G.; Li, Y.; Liu, H.; Guo, Y.; Li, Y.; Zhu, D. Architecture of Graphdiyne Nanoscale Films. *Chem. Commun.* **2010**, *46*, 3256−3258.
(27) Li, G. X.; Li, Y. L.; Qian, X. M.; Liu, H. B.; Lin, H. W.; Chen, N.; Li, Y. J. Construction of Tubular Molecule Aggregations of Graphdiyne for Highly Efficient Field Emission. *J. Phys. Chem. C* **2011**, *115*, 2611−2615.
(28) Zhou, J.; Gao, X.; Liu, R.; Xie, Z.; Yang, J.; Zhang, S.; Zhang, G.; Liu, H.; Li, Y.; Zhang, J.; Liu, Z. Synthesis of Graphdiyne Nanowalls Using Acetylenic Coupling Reaction. *J. Am. Chem. Soc.* **2015**, *137*, 7596−7599.
(29) Gao, X.; Zhou, J.; Du, R.; Xie, Z.; Deng, S.; Liu, R.; Liu, Z.; Zhang, J. Robust Superhydrophobic Foam: A Graphdiyne-Based Hierarchical Architecture for Oil/Water Separation. *Adv. Mater.* **2016**, *28*, 168−173.
(30) Ferrari, A. C.; Basko, D. M. Raman Spectroscopy as a Versatile Tool for Studying the Properties of Graphene. *Nat. Nanotechnol.* **2013**, *8*, 235−246.
(31) Cronin, S. B.; Swan, A. K.; Unlu, M. S.; Goldberg, B. B.; Dresselhaus, M. S.; Tinkham, M. Measuring the Uniaxial Strain of Individual Single-Wall Carbon Nanotubes: Resonance Raman Spectra of Atomic-Force-Microscope Modified Single-Wall Nanotubes. *Phys. Rev. Lett.* **2004**, *93*, 167401.
(32) Popov, V. N.; Lambin, P. Theoretical Raman Fingerprints of A-,B-, and Γ-Graphyne. *Phys. Rev. B: Condens. Matter Mater. Phys.* **2013**, *88*, 075427.
(33) Wang, J.; Zhang, S.; Zhou, J.; Liu, R.; Du, R.; Xu, H.; Liu, Z.; Zhang, J.; Liu, Z. Identifying Sp-Sp2 Carbon Materials by Raman and Infrared Spectroscopies. *Phys. Chem. Chem. Phys.* **2014**, *16*, 11303−11309.
(34) Bedell, S. W.; Khakifirooz, A.; Sadana, D. K. Strain Scaling for CMOS. *MRS Bull.* **2014**, *39*, 131−137.
(35) Hytch, M.; Houdellier, F.; Hue, F.; Snoeck, E. Nanoscale Holographic Interferometry for Strain Measurements in Electronic Devices. *Nature* **2008**, *453*, 1086−1089.
(36) Mohiuddin, T. M. G.; Lombardo, A.; Nair, R. R.; Bonetti, A.; Savini, G.; Jalil, R.; Bonini, N.; Basko, D. M.; Galiotis, C.; Marzari, N.; Novoselov, K. S.; Geim, A. K.; Ferrari, A. C. Uniaxial Strain in Graphene by Raman Spectroscopy: G Peak Splitting, Gruneisen Parameters, and Sample Orientation. *Phys. Rev. B: Condens. Matter Mater. Phys.* **2009**, *79*, 205433.
(37) Giannozzi, P.; et al. Quantum Espresso: A Modular and Open-Source Software Project for Quantum Simulations of Materials. *J. Phys.: Condens. Matter* **2009**, *21*, 395502.
(38) Baroni, S.; de Gironcoli, S.; Dal Corso, A.; Giannozzi, P. Phonons and Related Crystal Properties from Density-Functional Perturbation Theory. *Rev. Mod. Phys.* **2001**, *73*, 515−562.
(39) Mounet, N.; Marzari, N. First-Principles Determination of the Structural, Vibrational and Thermodynamic Properties of Diamond, Graphite, and Derivatives. *Phys. Rev. B: Condens. Matter Mater. Phys.* **2005**, *71*, 205214.
(40) Huang, H.; Duan, W.; Liu, Z. The Existence/Absence of Dirac Cones in Graphynes. *New J. Phys.* **2013**, *15*, 023004.
(41) Malko, D.; Neiss, C.; Vines, F.; Gorling, A. Competition for Graphene: Graphynes with Direction-Dependent Dirac Cones. *Phys. Rev. Lett.* **2012**, *108*, 086804.
(42) Pan, L. D.; Zhang, L. Z.; Song, B. Q.; Du, S. X.; Gao, H. J. Graphyne- and Graphdiyne-Based Nanoribbons: Density Functional Theory Calculations of Electronic Structures. *Appl. Phys. Lett.* **2011**, *98*, 173102.
(43) Narita, N.; Nagai, S.; Suzuki, S.; Nakao, K. Optimized Geometries and Electronic Structures of Graphyne and Its Family. *Phys. Rev. B: Condens. Matter Mater. Phys.* **1998**, *58*, 11009−11014.
(44) Malard, L. M.; Guimarães, M. H. D.; Mafra, D. L.; Mazzoni, M. S. C.; Jorio, A. Group-Theory Analysis of Electrons and Phonons In-Layer Graphene Systems. *Phys. Rev. B: Condens. Matter Mater. Phys.* **2009**, *79*, 125426.
(45) Porezag, D.; Pederson, M. R.; Frauenheim, T.; Köhler, T. Structure, Stability, and Vibrational Properties of Polymerized C_{60}. *Phys. Rev. B: Condens. Matter Mater. Phys.* **1995**, *52*, 14963−14970.

DOI: 10.1021/acs.jpcc.5b12388
J. Phys. Chem. C 2016, 120, 10605−10613

(46) Eichhorn, J.; Heckl, W. M.; Lackinger, M. On-Surface Polymerization of 1,4-Diethynylbenzene on Cu(111). *Chem. Commun. (Cambridge, U. K.)* **2013**, *49*, 2900−2902.
(47) Bauer, H.; Faust, J.; Froböse, R.; Füssel, J.; Krüerke, U.; Kunz, M.; Somer, H. M. *Cu Organocopper Compounds*; Springer-Verlag: Berlin, 1986.
(48) Hu, A.; Rybachuk, M.; Lu, Q. B.; Duley, W. W. Direct Synthesis of Sp-Bonded Carbon Chains on Graphite Surface by Femtosecond Laser Irradiation. *Appl. Phys. Lett.* **2007**, *91*, 131906.
(49) Hegelund, F.; et al. The Harmonic Force Field and Ground-State Average Structure of Allene. *J. Mol. Spectrosc.* **1977**, *65*, 366−378.
(50) Kurti, J.; Magyar, C.; Balazs, A.; Rajczy, P. Vibrational Analysis for Short Carbon Chains with Alternating and Cumulenic Structure. *Synth. Met.* **1995**, *71*, 1865−1866.
(51) Yuan, Q.; Ding, F. Formation of Carbyne and Graphyne on Transition Metal Surfaces. *Nanoscale* **2014**, *6*, 12727−12731.
(52) Cao, G. Atomistic Studies of Mechanical Properties of Graphene. *Polymers* **2014**, *6*, 2404−2432.
(53) Nye, J. F. *Physical Properties of Crystals*; Oxford Science Publications: Oxford, 1995.
(54) Lee, C.; Wei, X.; Kysar, J. W.; Hone, J. Measurement of the Elastic Properties and Intrinsic Strength of Monolayer Graphene. *Science* **2008**, *321*, 385−388.
(55) Wei, X.; Fragneaud, B.; Marianetti, C. A.; Kysar, J. W. Nonlinear Elastic Behavior of Graphene:Ab Initiocalculations to Continuum Description. *Phys. Rev. B: Condens. Matter Mater. Phys.* **2009**, *80*, 205407.
(56) Andrew, R. C.; Mapasha, R. E.; Ukpong, A. M.; Chetty, N. Mechanical Properties of Graphene and Boronitrene. *Phys. Rev. B: Condens. Matter Mater. Phys.* **2012**, *85*, 125428.
(57) Mohiuddin, T. M. G.; Lombardo, A.; Nair, R. R.; Bonetti, A.; Savini, G.; Jalil, R.; Bonini, N.; Basko, D. M.; Galiotis, C.; Marzari, N.; Novoselov, K. S.; Geim, A. K.; Ferrari, A. C. Uniaxial Strain in Graphene by Raman Spectroscopy: G Peak Splitting, Gruneisen Parameters, and Sample Orientation. *Phys. Rev. B: Condens. Matter Mater. Phys.* **2009**, *79*, 205433.
(58) Huang, M.; Yan, H.; Chen, C.; Song, D.; Heinz, T. F.; Hone, J. Phonon Softening and Crystallographic Orientation of Strained Graphene Studied by Raman Spectroscopy. *Proc. Natl. Acad. Sci. U. S. A.* **2009**, *106*, 7304−7308.
(59) Mohr, M.; Papagelis, K.; Maultzsch, J.; Thomsen, C. Two-Dimensional Electronic and Vibrational Band Structure of Uniaxially Strained Graphene Fromab Initiocalculations. *Phys. Rev. B: Condens. Matter Mater. Phys.* **2009**, *80*, 205410.
(60) Bissett, M. A.; Izumida, W.; Saito, R.; Ago, H. Effect of Domain Boundaries on the Raman Spectra of Mechanically Strained Graphene. *ACS Nano* **2012**, *6*, 10229−10238.
(61) Dion, M.; Rydberg, H.; Schroder, E.; Langreth, D. C.; Lundqvist, B. I. Van Der Waals Density Functional for General Geometries. *Phys. Rev. Lett.* **2004**, *92*, 246401.
(62) Liu, H.-L.; Siregar, S.; Hasdeo, E. H.; Kumamoto, Y.; Shen, C.-C.; Cheng, C.-C.; Li, L.-J.; Saito, R.; Kawata, S. Deep-Ultraviolet Raman Scattering Studies of Monolayer Graphene Thin Films. *Carbon* **2015**, *81*, 807−813.

DOI: 10.1021/acs.jpcc.5b12388
J. Phys. Chem. C 2016, 120, 10605−10613